# *E*-Plane Integrated Circuit Filters with Improved Stopband Attenuation

FRITZ ARNDT, SENIOR MEMBER, IEEE, JENS BORNEMANN, RÜDIGER VAHLDIECK, AND DIETRICH GRAUERHOLZ

***Abstract*—Improved stopband attenuation is achieved by thick strips, by reduced waveguide sidewall dimensions, and by double planar integrated circuits. In contrast to thick strips which may cause high passband insertion losses, and filters with reduced waveguide dimensions which require additional tapers, double planar *E*-plane integrated circuit filters combine the advantages of low costs, high stopband, and low passband insertion losses. Computer-aided design of a four-resonator *Ka*-band double metal insert filter achieves a calculated stopband attenuation between 40 and 60 GHz of more than 50 dB, the calculated minimum passband insertion loss is 0.43 dB (measured 1.8 dB). Higher order mode excitation and finite thicknesses of the inserts are included in the calculations.**

## I. Introduction and Formulation of Problem

Millimeter-wave *E*-plane integrated low insertion-loss filters (Fig. 1) may be designed by a) large-gap finlines, by which the high-$Q$ potential of finlines increasing with gapwidth is fully utilized [1]–[3]. Pure metal inserts b), mounted in the *E*-plane of rectangular waveguides requiring no supporting dielectrics, achieve still lower passband insertion losses [4]–[6].

The filter portions with metal strips or vertical fins are below the cutoff frequency for fundamental-mode operation if the filter is operated within the waveguide band for which it is designed. The resonators are coupled by way of evanescent fields along the strips, which show inductive behavior. For higher operating frequencies than the waveguide band—especially for designs in the near of the waveguide band end— however, attainable stopband attenuation and edge steepness may be too low for many purposes, e.g., for diplexers.

This is demonstrated in Fig. 2, where the typical insertion loss of a conventional three-resonator *Ka*-band finline filter [6] is shown. The passband is centered at 39 GHz,. The insertion loss at, e.g., 43 GHz, is only about 37 dB. The reason is that, beyond the cutoff frequency within the strip sections, the power is increasingly transported directly by then propagating waves along the strip section which destroy the filter behavior of the inductive strip-coupled resonators.

This paper discusses some proposals to overcome this problem. These will include the introduction of a double planar *E*-plane integrated circuit filter which combines the advantages of low cost, high stopband, and low passband insertion-loss designs. Computer-optimized filter data for a *Ka*-band prototype will be given and proved by measurements.

## II. Thick Inserts

A first possibility to improve stopband attenuation is to reduce the distance between the strips and the waveguide sidewalls by thick dielectric substrates or thick metal inserts. Since thick dielectrics cause considerable additional losses, a pure-metal insert filter is chosen for design example with 2-mm-thick inserts and three resonators. Computer-aided design is used according to [5], the filter data are given in Table I. For the examples listed in Table I, the 3-dB bandwidths are chosen to be about $0.5,\cdots,1.2$ percent since the *E*-plane metal insert technique [4]–[6] typically

Manuscript received September 14, 1983; revised April 9, 1984.

The authors are with the Microwave Department, University of Bremen, Kufsteiner Str., NW 1, D-2800 Bremen 33, West Germany.

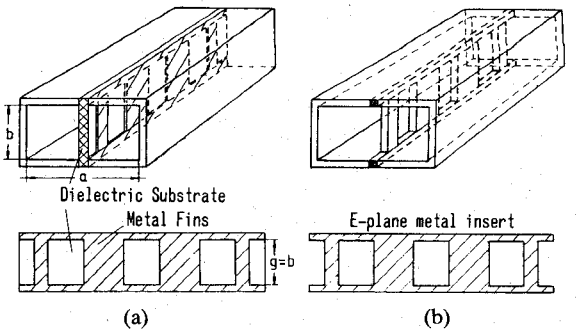


Fig. 1. Millimeter-wave *E*-plane integrated low-insertion-loss filters, (a) large gap finlines, (b) pure metal inserts.

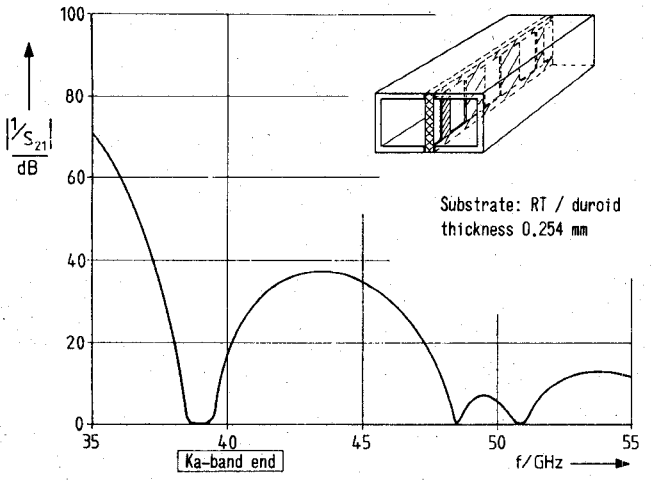


Fig. 2. Insertion-loss of a conventional three-resonator *Ka*-band finline filter [6] with passband at about 39 GHz. Data according to [6], analyzed with the theory of [2], [3].

yields appropriate narrow-band filters. In principle, higher bandwidths are possible, but this property has to be considered carefully against other requirements, concerning, e.g., passband ripple, number of resonators (which influences considerably passband insertion loss due to copper losses), edge steepness, and attainable stopband attenuation levels.

The 2-mm-thick metal insert filter achieves good stopband behavior, as is indicated in Fig. 3, but a disadvantage is also quite evident: measured high passband insertion loss, as shown in the detail picture. This may result from grounding difficulties or sharp edges on strips; also, mechanical tolerances may lead to an inappropriate staggering of the single resonant circuits of the filter. This is illustrated in the right-hand illustration. The typical filing tolerances of about 0.05 mm are included in the computations (dashed line), while the insertion loss is about 2 dB.

## III. *Ka*-Band Filter within *Q*-Band Waveguide

A second way to reduce the critical distance between the metal inserts and the waveguide sidewalls is to reduce the sidewall distance itself. This solution is indicated in Fig. 4, where a four-resonator *Ka*-band metal insert filter is shown, designed according to [5] for the housing of the next higher waveguide band—the *Q*-band— with two 50-mm-long linear taper-sections to the *Ka*-band waveguide. The return loss of the tapers is greater than 35 dB within *Q*-band, as has been calculated by field theory analysis in [7].

The design data of the filter are given in Table I. As can be seen in Fig. 4, the stopband behavior is excellent, the measured

0018-9480/84/1000-1391$01.00 ©1984 IEEE

TABLE I
COMPUTER-OPTIMIZED DESIGN DATA FOR HIGH STOPBAND ATTENUATION *E*-PLANE METAL INSERT FILTERS

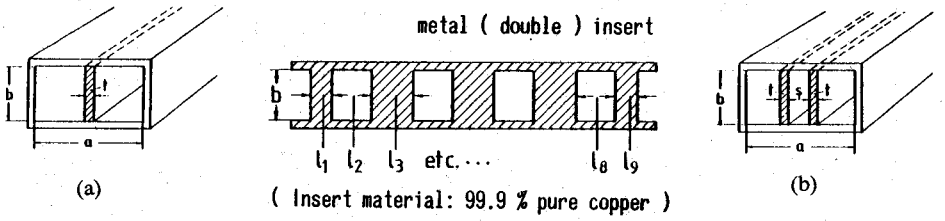


| Frequency-band for the filter design / waveguide housing | Number of resonators | Design type | Insert thickness t ( mm ) / spacing s ( mm ) | $l_1 = l_9$ ( mm ) | $l_2 = l_8$ ( mm ) | $l_3 = l_7$ ( mm ) | $l_4 = l_6$ ( mm ) | $l_5$ ( mm ) | Midband-frequency ( GHz ) | 3 dB-band-width ( GHz ) | min.passband insertion-loss ( dB ) |
|---|---|---|---|---|---|---|---|---|---|---|---|
| Ka - band<br>a = 7.112 mm<br>b = 3.556 mm<br>WR 28 | 3 | a single insert | t = 2.0 | 0.787 | 4.023 | 3.461 | 4.028 | | 39.5 | 0.5 | 0.1<br>2 mech. tolerances included |
| Ka - band<br>a = 5.689 mm<br>b = 2.845 mm<br>WR 22 | 4 | a single insert | t = 0.2 | 1.044 | 3.890 | 3.524 | 3.900 | 3.938 | 39.5 | 0.4 | 0.003 |
| Ka - band<br>a = 7.112 mm<br>b = 3.556 mm<br>WR 28 | 4 | b double insert | t = 0.15<br>s = 1.8 | 0.403 | 3.637 | 2.448 | 3.689 | 3.646 | 39.5 | 0.2 | 0.43 |
| | | | | $l_1$ = 0.420<br>$l_9$ = 0.400 | $l_2$ = 3.660<br>$l_8$ = 3.665 | $l_3$ = 2.420<br>$l_7$ = 2.420 | $l_4$ = 3.735<br>$l_6$ = 3.710 | $l_5$ = 3.590 | 39.04 | 0.2 | 1.8 mech. tolerances included |
| | | | | $l_1$ = 0.400<br>$l_9$ = 0.400 | $l_2$ = 3.630<br>$l_8$ = 3.640 | $l_3$ = 2.430<br>$l_7$ = 2.425 | $l_4$ = 3.695<br>$l_6$ = 3.700 | $l_5$ = 3.625 | | | |

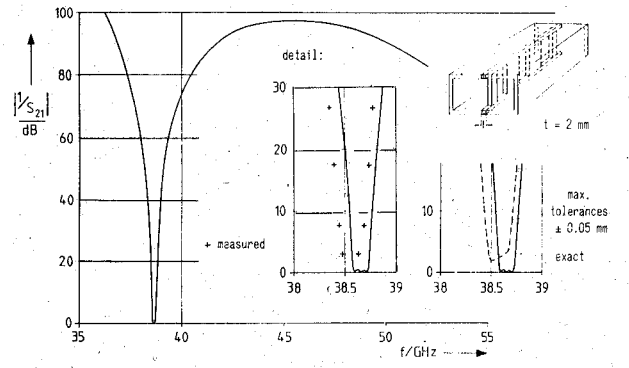


Fig. 3. Calculated and measured insertion loss of a *Ka*-band metal insert filter with 2-mm-thick metal insert and three resonators, data see Table I.

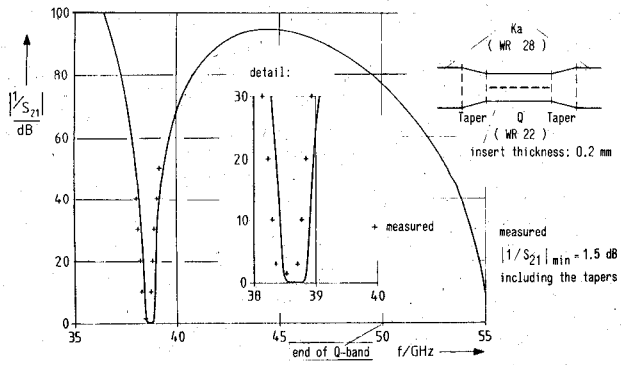


Fig. 4. Calculated and measured insertion loss of a *Ka*-band metal-insert filter within *Q*-band waveguide housing. The linear tapers are 50 mm long.

minimum passband insertion loss is 1.5 dB, including the tapers. Because of the mechanical efforts concerning the taper sections, however, this filter type does not achieve low-cost design and thus offsets one of the typical advantages of the *E*-plane integrated circuit filters in comparison with conventional waveguide filters.

## IV. DOUBLE PLANAR INTEGRATED CIRCUIT FILTER

The filter design which combines all the advantages (low costs, low tolerance etching techniques, low passband, high stopband insertion loss, low losses because of the absence of dielectrics) is the double planar integrated circuit filter, where two metal inserts are mounted in the *E*-plane of the waveguide, as shown in Fig. 5.

### *A. Theory*

Similar to the single metal insert filter [5], the design of optimized double metal inserts is based on field expansion into suitable orthogonal eigenmodes in the subregions, together with field matching at common interfaces at the steps investigated. This allows inclusion of the higher order mode excitation up to a desired number of modes and the finite thickness of the metallic strips.

For each subregion $\nu$ = I, II, III, IV (Fig. 5), the fields

$$\vec{E}^{(\nu)} = -j\omega\mu\nabla \times \vec{\Pi}_{hx}^{(\nu)}, \vec{H}^{(\nu)} = \nabla \times \nabla \times \vec{\Pi}_{hx}^{(\nu)} \qquad (1)$$

are derived from the $x$-component of the magnetic Hertzian vector $\vec{\Pi}_h$, which is assumed to be a sum of the eigenmodes satisfying the wave equation and the boundary conditions at the metallic surfaces at $x = 0$, $c$, $d$, $e$, $f$, and $a$:

$$\Pi_{hx}^{(\nu)} = \sum_{m=1}^{\infty} A_m^{(\nu)\pm} \cdot T_m^{(\nu)} \cdot \sin\left[\frac{m\pi}{p^{(\nu)}} \cdot f^{(\nu)}\right] \cdot e^{\mp jk_{zm}^{(\nu)} z} \qquad (2)$$

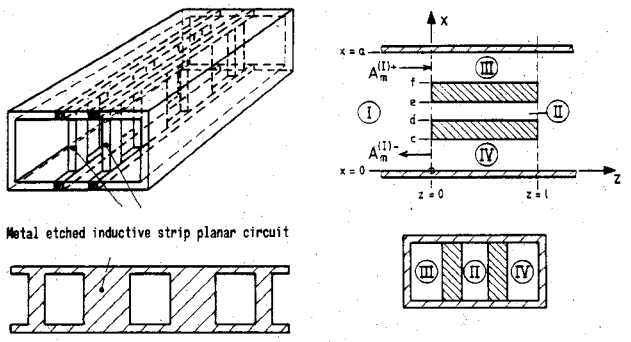


Fig. 5. Double-planar $E$-plane integrated circuit filter.

with

$$T_m^{(\nu)} = \frac{1}{k_{zm}^{(\nu)}\sqrt{\omega\mu k_{zm}^{(\nu)}}} \cdot \begin{cases} \sqrt{\dfrac{2}{ab}}, & \nu = \text{I} \\ \sqrt{\dfrac{2}{bc}}, & \nu = \text{IV} \\ \sqrt{\dfrac{2}{(e-d)b}}, & \nu = \text{II} \\ \sqrt{\dfrac{2}{(a-f)b}}, & \nu = \text{III} \end{cases} \tag{3}$$

$$(f^{(\nu)})' = (x, e-x, a-x, x); (p^{(\nu)})' = (a, e-d, a-f, c) \tag{4}$$

$$k_{zm}^{(\nu)} = \sqrt{k^2 - \left(\frac{m\pi}{p^{(\nu)}}\right)^2}, \qquad k^2 = \omega^2\mu\epsilon. \tag{5}$$

$A_m^{(\nu)\pm}$ are the still-unknown eigenmode amplitudes of the forward and backward waves which are suitably normalized by $T_m^{(\nu)}$ so that the power carried by a given wave is 1 W for a wave-amplitude coefficient of $\sqrt{1\text{W}}$.

By matching the tangential field components at the corresponding interfaces, the coefficients in (2) are determined after multiplication with the appropriate orthogonal function which leads to the corresponding coupling integrals given in the Appendix. This yields the four-port scattering matrix $(S)_{z=0}$ at the step discontinuity $z = 0$ (Fig. 5)

$$\begin{pmatrix} A^{(\text{I})-} \\ A^{(\text{III})+} \\ A^{(\text{II})+} \\ A^{(\text{IV})+} \end{pmatrix} = (S)_{z=0} \begin{pmatrix} A^{(\text{I})+} \\ A^{(\text{III})-} \\ A^{(\text{II})-} \\ A^{(\text{IV})-} \end{pmatrix}. \tag{6}$$

The step discontinuity at $z = l$ (Fig. 5) can be treated in a similar manner. The overall two-port scattering matrix $(S)$ of the discontinuity waveguide to section of metal $E$-plane bar and back to waveguide is given by

$$\begin{pmatrix} A^{(\text{I})-} \\ B^{(\text{I})+} \end{pmatrix} = (S) \begin{pmatrix} A^{(\text{I})+} \\ B^{(\text{I})-} \end{pmatrix} \tag{7}$$

where the coefficients of the scattering matrix are explained in the Appendix.

The scattering matrix of the total metal insert filter is then calculated by directly combining the single scattering matrices, like in [7]. Compared with the commonly used multiplication of transmission matrices, this procedure preserves numerical accuracy, since the direct combination of scattering matrix parameters contains exponential functions with only negative arguments.

For computer optimization, the expansion into nine eigenmodes at each discontinuity has turned out to be sufficient. The final design data are provided by forty-five eigenmodes.

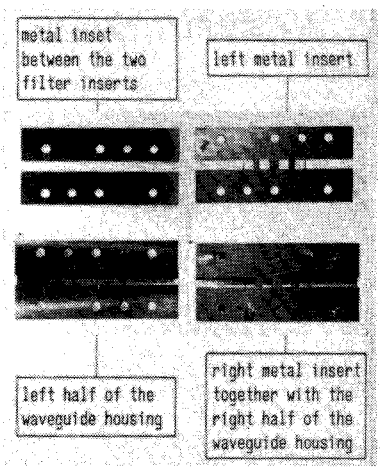


Fig. 6. Photograph of the optimized metal-etched double-planar $E$-plane integrated circuit $Ka$-band filter, design data see Table I.

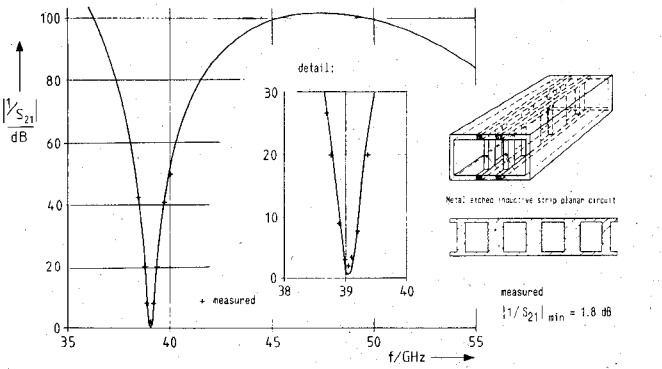


Fig. 7. Calculated and measured insertion loss of the optimized $Ka$-band four-resonator double-planar $E$-plane integrated circuit filter, design data see Table I.

### B. Design and Results

An optimizing computer program varies the $E$-plane metal strip lengths for given waveguide housing dimensions, number of resonators, metal insert thickness, and spacing, until the insertion loss within passband yields a minimum and the stopband attenuation an optimum. The design data of a $Ka$-band four-resonator double integrated circuit filter prototype are given in Table I. The tolerances of the metal-etched double insert dimensions in relation to the optimized data are about $\pm 20$ $\mu$m, as has been checked by a measuring microscope. The material of the inserts is 99.9-percent pure copper. Fig. 6 shows the photograph of the filter structures together with the opened waveguide housing. The metal inset between the two filter inserts is 1.8 mm thick. The metal insert thickness of the two filter circuits is 0.15 mm.

Fig. 7 shows the calculated and measured insertion loss of the optimized double integrated circuit filter. The measured minimum insertion loss is 1.8 dB, the calculated stopband attenuation between 40 and 60 GHz is more than about 50 dB.

## V. Conclusion

Improvement of the stopband behavior of $E$-plane circuit filters is possible by thick strips, by reducing the waveguide sidewall dimensions, and by double planar integrated circuits. Thick strips may cause high passband insertion loss; reduced waveguide sidewall dimensions require additional taper sections, which increase the costs. The design which combines the advantages of high stopband attenuation, low passband insertion loss, low costs, and low tolerances by metal etching is the double-planar integrated circuit filter. A $Ka$-band four-resonator computer-optimized prototype achieves a calculated stopband

attenuation of more than 50 dB for 40 to 60 GHz, the measured minimum insertion loss is 1.8 dB. Since the higher order mode excitation and finite thickness of the insert are included in the calculations, the measurements agree well with theory.

## Appendix

### Coupling Integrals due to the Orthogonal Expansion

$$F^{\mathrm{IV}}_{(mn)} = \int_0^c \sin\left(\frac{m\pi}{a}x\right)\sin\left(\frac{n\pi}{c}y\right)dx$$

$$F^{\mathrm{III}}_{(mq)} = \int_f^a \sin\left(\frac{m\pi}{a}x\right)\sin\left(\frac{q\pi}{a-f}\cdot(x-f)\right)dx$$

$$F^{\mathrm{II}}_{(mk)} = \int_d^e \sin\left(\frac{m\pi}{a}x\right)\sin\left(\frac{k\pi}{e-d}\cdot(x-d)\right)dx.$$

### Scattering Coefficients in (6)

$$(S)_{11} = (S)_{12} = \left\{I+U-W(I+U)^{-1}W\right\}^{-1} \cdot \left\{I-U-W(I+U)^{-1}W\right\}$$

$$(S)_{12} = (S)_{21} = \left\{I+U-W(I+U)^{-1}W\right\}^{-1} \cdot W\left\{U-(I+U)^{-1}(I-U)\right\}$$

where

$$I = \sum_{\nu=\mathrm{II}}^{\mathrm{IV}} L^{\nu}_E\left\{U+2D^{\nu}(U-D^{\nu}D^{\nu})^{-1}D^{\nu}\right\}L^{\nu}_H$$

$$W = \sum_{\nu=\mathrm{II}}^{\mathrm{IV}} 2L^{\nu}_E D^{\nu}(U-D^{\nu}D^{\nu})^{-1}L^{\nu}_H$$

with

$U$ unit matrix,

$D^{\nu}$ diagonal matrix of the eigenmodes (also below their cutoff frequency) along the waveguide sections $i$ between the step discontinuities

$$D^{\nu}_{(mm)} = e^{-jk^{\nu}_{z(m)}\cdot l_i}$$

$$L^{\mathrm{IV}}_{E(mn)} = 2\sqrt{\frac{k^{\mathrm{I}}_{z(m)}}{a\cdot c\cdot k^{\mathrm{IV}}_{z(n)}}}\cdot F^{\mathrm{IV}}_{(mn)}$$

$$L^{\mathrm{II}}_{E(mk)} = 2\sqrt{\frac{k^{\mathrm{I}}_{z(m)}}{a(e-d)k^{\mathrm{II}}_{z(k)}}}\cdot F^{\mathrm{II}}_{(mk)}$$

$$L^{\mathrm{III}}_{E(mq)} = 2\sqrt{\frac{k^{\mathrm{I}}_{z(m)}}{a(a-f)k^{\mathrm{III}}_{z(q)}}}\cdot F^{\mathrm{III}}_{(mq)}$$

$$(L^{\nu}_H) = (L^{\nu}_E)^T, (T = \text{transposed}).$$

## Acknowledgment

The authors wish to thank Dr. Rembold, the head of the microwave laboratory of AEG Telefunken, Ulm, West Germany, and the members of his staff, especially Dr. Menzel, for helpful discussions and financial support of this work.

## References

[1] P. J. Meier, "Integrated fin-line millimeter components," *IEEE Trans. Microwave Theory Tech.*, vol. MTT-22, pp. 1209–1216, Dec. 1974.

[2] F. Arndt, J. Bornemann, D. Grauerholz, and R. Vahldieck, "Low-insertion loss fin-line filters for millimeter-wave applications," in *Proc. 11th European Microwave Conf.*, Amsterdam, 1981, pp. 309–314.

[3] ———, "Theory and design of low-insertion loss fin-line filters," *IEEE Trans. Microwave Theory Tech.*, vol. MTT-30, pp. 155–163, Feb. 1982.

[4] Y. Konishi and K. Uenakada, "The design of a bandpass-filter with inductive strip—Planar circuit mounted in waveguide," *IEEE Trans. Microwave Theory Tech.*, vol. MTT-22, pp. 869–873, Oct. 1974.

[5] R. Vahldieck, J. Bornemann, F. Arndt, and D. Grauerholz, "Optimized waveguide *E*-plane metal insert filters for millimeter-wave applications," *IEEE Trans. Microwave Theory Tech.*, vol. MTT-31, pp. 65–69, Jan. 1983.

[6] Y.-C. Shi, T. Itoh, and L. Q. Bui, "Computer-aided design of millimeter-wave *E*-plane filters," *IEEE Trans. Microwave Theory Tech.*, vol. MTT-31, pp. 135–141, Feb. 1983.

[7] H. Patzelt and F. Arndt, "Double-plane steps in rectangular waveguides and their application for transformers, irises, and filters," *IEEE Trans. Microwave Theory Tech.*, vol. MTT-30, pp. 771–776, May 1982.

# A Comparison of IMPATT Oscillator Power and Frequency Above 100 GHz with Results Derived from Theoretical Models

BEVAN D. BATES, MEMBER, IEEE

***Abstract*—A comparison is made of experimentally determined IMPATT oscillator frequency and power characteristics in the 90–140-GHz band with values obtained from detailed theoretical models. The results show encouraging agreement and demonstrate the potential of the modeling approach for oscillator design.**

## I. Introduction

This paper compares measured 117-GHz IMPATT oscillator frequency and output power with results derived from theoretical circuit models. Previous millimeter-wave oscillator models reported in the literature either rely on small-signal device models [1], [2] and therefore cannot yield output power, or use elementary circuit models [3] and are thus unsuitable for studying circuit behavior, such as oscillator tuning as a function of waveguide short position or other circuit parameters. In this paper, oscillator circuit modeling techniques, successfully applied at *X*-band [4], [5], are applied for the first time to a millimeter-wave IMPATT oscillator circuit.

## II. Oscillator Circuit Description

The circuit under consideration, shown in Fig. 1, is of the cross-coupled coaxial/waveguide type, constructed in half-height waveguide with a linearly tapered transition to full-height waveguide at the output. The IMPATT diode, mounted on a copper heatsink in a double-quartz-standoff package, is soldered to a copper post and inserted in the lower coaxial section and contacted by the coaxial center conductor. The other end of the coaxial line is terminated at RF by a section of Eccosorb[1]

Manuscript received October 24, 1983; revised April 13, 1984. This work was supported by a National Research Council Resident Research Associateship at the Jet Propulsion Laboratory, Pasadena, CA, under contract with the National Aeronautics and Space Administration.

The author is with the Department of Electrical and Electronic Engineering, University of Melbourne, Parkville, Vic., 3052, Australia. He was an NRC-NASA Resident Research Associate at the Jet Propulsion Laboratory, 4800 Oak Grove Drive, Pasadena, CA 91109.

[1]Emerson and Cuming, Inc

0018-9480/84/1000-1394$01.00 ©1984 IEEE